A numerical study of the run-up generated by three-dimensional landslides

Patrick Lynett
Department of Civil Engineering, Texas A&M University, College Station, Texas, USA

Philip L.-F. Liu
School of Civil and Environmental Engineering, Cornell University, Ithaca, New York, USA

Received 18 March 2004; revised 20 October 2004; accepted 19 January 2005; published 8 March 2005.

[1] A large set of numerical experiments are designed to examine the maximum run-up generated by three-dimensional (3-D) submerged and subaerial, solid body landslides. A depth-integrated numerical model is utilized, allowing for the efficient simulation of landslides in shallow and intermediate water. Six dimensionless parameters are introduced: the slide thickness, the slide wave number, a slide shape parameter, the horizontal aspect ratio of the slide, the specific gravity of the slide mass, and the slope of the beach. Six sets of simulations are first presented, wherein one of the six dimensionless parameters are singularly varied. This allows for the identification of parameter dependence on maximum run-up. After combining the dependencies a number of relationships appear. Most notably, a very clear division between the near and far field is observed, where here the far field is defined as the region displaced from the projection of the landslide, on the nearby beach, where edge waves may dominate the wave pattern. For submerged slides a nondimensional estimation of the maximum run-up just landward of the slide is found as well as the location and magnitude of the secondary run-up peak. This secondary peak is due to the propagation of edge waves and is in some cases larger than the peak immediately landward of the slide. The results presented in this paper may be useful for preliminary hazard assessment, where a simple and quick estimation of the maximum run-up height and locations are required. Additionally, the formulas developed will be particularly beneficial to those developing 3-D landslide experiments.

Citation: Lynett, P., and P. L.-F. Liu (2005), A numerical study of the run-up generated by three-dimensional landslides, *J. Geophys. Res.*, *110*, C03006, doi:10.1029/2004JC002443.

1. Introduction

[2] Interest in landslide generated tsunamis has risen in the last decade, due in large part to the devastating slump-induced tsunami of Papua New Guinea (PNG) in 1998 [e.g., *Synolakis et al.*, 2002]. Additionally, in parts of the United States, mainly on the west coast, significant efforts have been recently undertaken to assess landslide tsunami hazards. Landslide tsunamis tend to be local, although possibly extreme, in their effects. Recorded on-land water elevations for the PNG tsunami exceed 10 m, but this large wave height was restricted to a shoreline length of roughly 15 km.

[3] Landslide tsunamis require a different characterization than earthquake tsunamis due to the fact that the length scale of a landslide, and the resulting tsunami, is typically much less than that of an earthquake. The physical implication of this fact is that, although described by the long wave descriptor tsunami, landslide tsunamis are not necessarily best characterized as long waves. Recent numerical work has shown that for typical submarine landslide setups, frequency dispersion can play an important role in determining both the offshore wave field and the shoreline movement [e.g., *Lynett and Liu*, 2002; *Lynett et al.*, 2003].

[4] To date, very few studies of landslide generated tsunamis include two horizontal dimension (2HD) effects. Numerically, although there are numerous 2HD landslide model presentations [e.g., *Jiang and LeBlond*, 1994; *Grilli et al.*, 2002] there is little in the way of model application for tsunami characterization. One such recent effort to look at 2HD slide tsunamis is that of *Okal and Synolakis* [2004], who used run-up distributions to infer characteristics of the source. The work to be presented here is similar in nature, although the focus is on a more complete landslide model, while the work of *Okal and Synolakis* [2004] also consider dislocation sources.

[5] 2HD landslide tsunami studies are particularly daunting, because of difficultly in minimizing reflection off three tank walls, such that uncontaminated run-up measurements can be obtained. Despite this hurdle, recent experiments [*Synolakis and Raichlen*, 2002] have been performed with a tank width of four slide widths. This type of experiment

0148-0227/05/2004JC002443$09.00

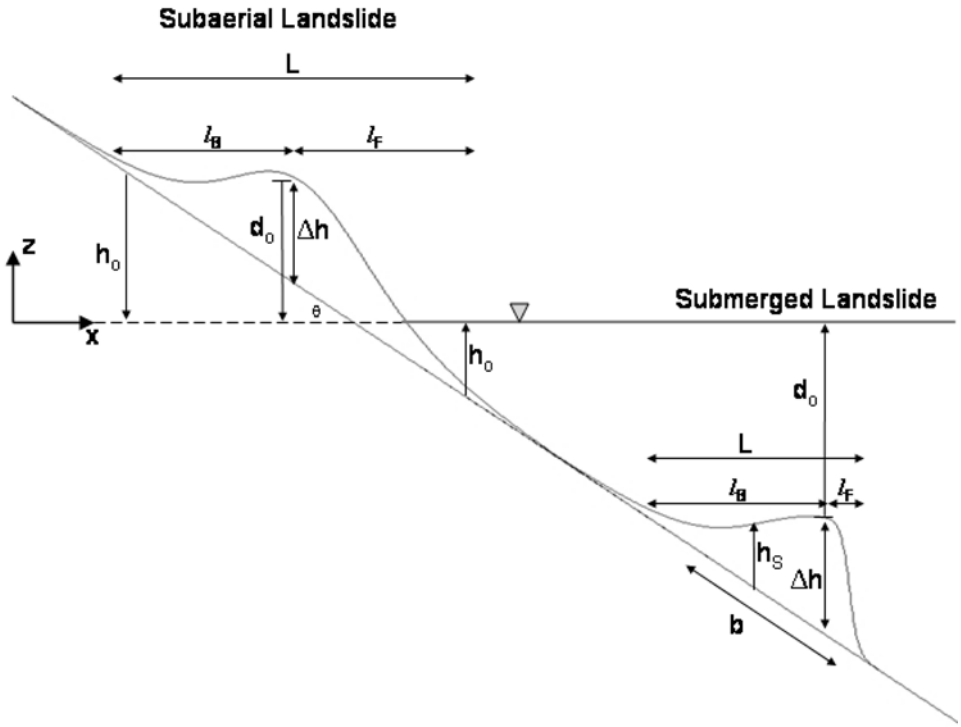

Figure 1. Definitions for a (left) subaerial and (right) submerged sliding mass. Note that the subaerial slide is symmetric in the horizontal plane ($\kappa = l_F/l_B = 1$), while the submerged slide is not ($\kappa \approx 0.15$).

allows for detailed physical study of the leading tsunami waves, but wall reflections quickly contaminate secondary behavior. Without examination of the secondary behavior, it becomes possible to miss one of the important phenomena controlling landslide tsunami run-up: edge waves.

[6] Edge waves have been studied by coastal engineers and scientists for many decades, largely motivated by *Ursell*'s [1952] analytical solution for edge waves on a constant slope. Edge waves, while rarely observed directly in typical coastal environments [*Schaffer and Jonsson*, 1992], can be easily discriminated for transient disturbances, such as tsunamis [*Gonzalez et al.*, 1995]. It seems reasonable to expect that submerged landslide tsunamis, and especially subaerial landslide tsunamis, with their fair amount of oblique wave energy, would generate shore-trapped, edge wave modes. In fact, this expectation has already been observed in experimental testing [e.g., *Liu et al.*, 1994; *Chang*, 1995] and numerical simulation of landslide tsunamis [e.g., *Tinti et al.*, 1999].

[7] This paper is organized as follows. First, a description of the theoretical model to be used is presented, followed by the method of numerical simulation. Next, the landslide geometry and motion profiles are given. It is in this section that the nondimensional parameters governing the physical slide characteristics are developed. After the setup description, results from the numerical simulations are examined. For each of the six nondimensional parameters, a subset of simulations is run, varying that parameter while holding the other five constant. Finally, all of the scaling laws extracted from the six subsets of simulations are combined, yielding global scalings.

2. Model Equations

[8] The model to be applied here is the 2HD, depth-integrated, multilayer model. The multilayer concept represents a different approach to developing a depth-integrated model with high-order dispersive properties. The multilayer derivation consists of a piecewise integration of the primitive equations of motion through N constant-density layers of arbitrary thickness. Within each layer, an independent velocity profile is determined. With N separate velocity profiles, matched at the interfaces of the layers, the resulting set of equations have $N + 1$ free parameters, allowing for an optimization with known analytical properties of water waves. The optimized two-layer model equations, which are used in the study presented here, show good linear wave characteristics up to $kh \approx 8$, while the second-order nonlinear behavior is well captured to $kh \approx 6$. Details of the multilayer approach can be found in the work of *Lynett* [2002] (see http://ceprofs.tamu.edu/plynett/publications/publications.htm) and *Lynett and Liu* [2004a, 2004b], while applications can be found in the work of *Basterretxea et al.* [2004] and *Ryu et al.* [2003]. The layer interface and the characteristic velocity elevations are specified as functions of the water depth, and thus these elevations change in time with the moving seafloor. On initially dry land, all of the layer elevations converge on $z = -h$ and are not allowed to exist below the beach. Thus on initially dry land, the two-

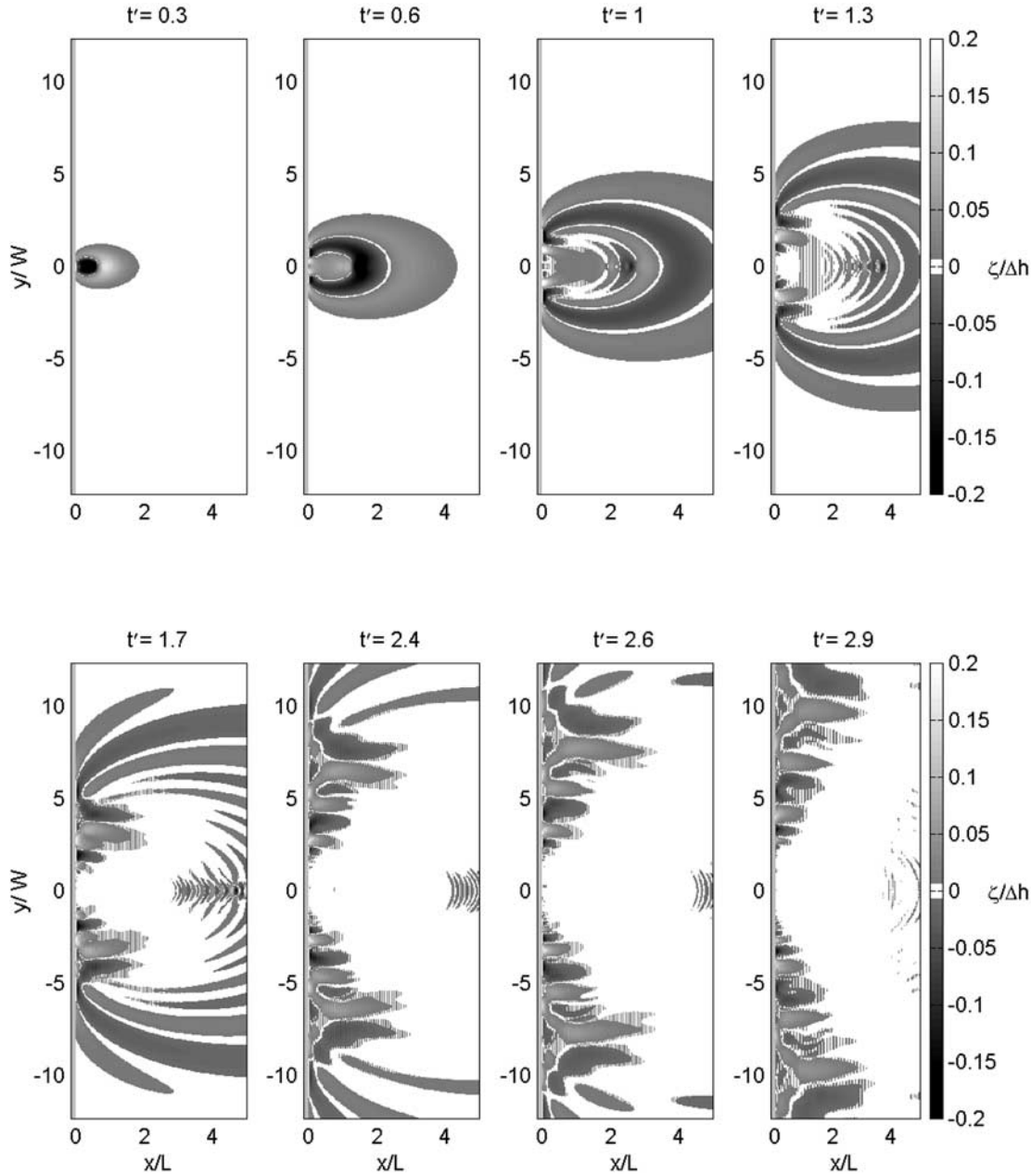

Figure 2. Spatial snapshots of the free surface.

layer model reduces to the one-layer model with the velocity evaluation level at the seabed.

[9] The simplest of the multilayer models is the one-layer model, which is equivalent to the model of *Liu* [1994] and the fully nonlinear extension of *Nwogu*'s [1993] model presented by *Wei et al.* [1995]. An analysis of the one-layer model's ability to predict the waves created by submarine landslides was done by *Lynett and Liu* [2002]. All of the accuracy restrictions given in that paper, in the form of minimum initial slide length scale to depth of submergence ratios, were closely followed in this study.

[10] As the one-layer accuracy restrictions are enforced in all the simulations performed, the obvious question of "why use the two-layer model" arises. The answer is that the two-layer model is required to overcome the practical and numerical challenges of these simulations. The primary difference between the one- and two-layer model is that the two-layer model is accurate into much deeper water, in both the linear and nonlinear sense. It was found from numerical testing that if the landslide was stopped, slowed, allowed to exit the numerical domain, or travel onto a milder slope, waves would be generated by this change. These waves would affect the run-up patterns, essentially contaminating the results with a small, but unknown error. Thus for the desired outcome of run-up generated by a slide traveling down a slope, the slope and the slide motion needed to be continuous and uninterrupted for the entire duration of each numerical simulation. While this objective may seem trivial or obvious from a numerical setup point of

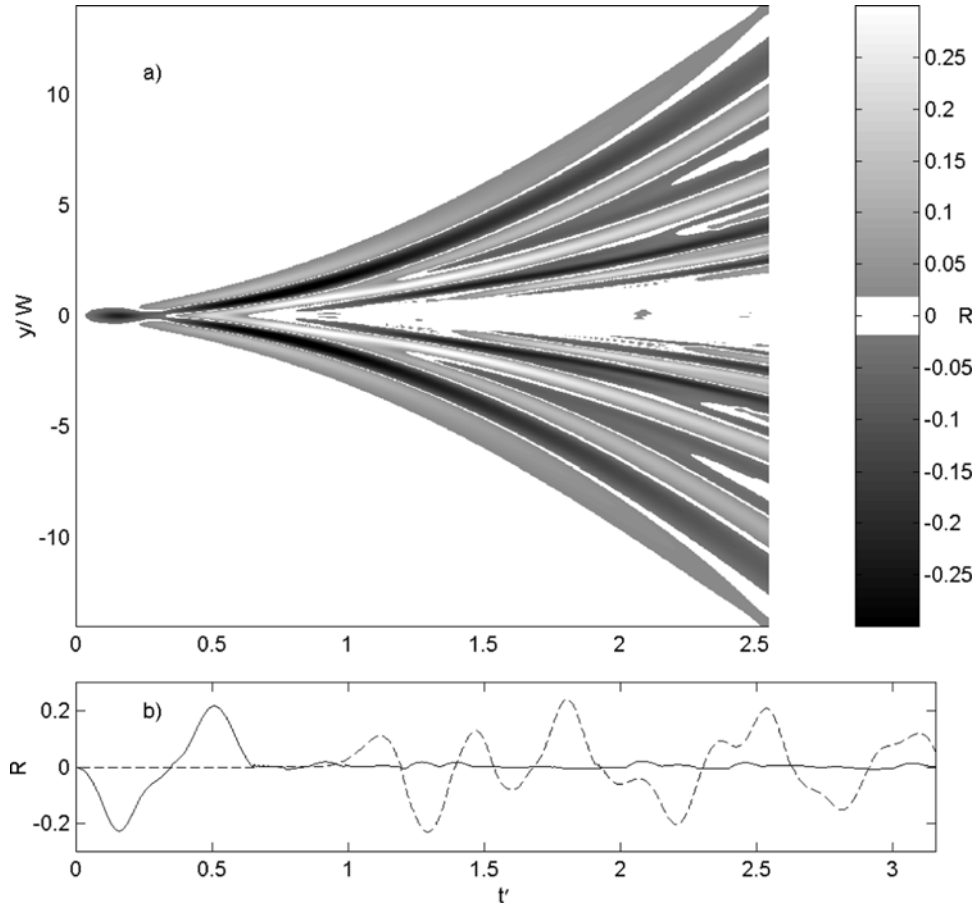

Figure 3. (a) Shoreline elevation as a function of time and transverse coordinate. (b) Run-up time series at $y/W = 0$ (solid line) and $y/W = 3$ (dashed line).

view, it is in fact not. The one-layer (Boussinesq) model, applied to deep water, tends to become unstable, predicting very large, rapidly (and unphysically) propagating short waves. These short waves will typically lead to numerical instability. When attempting to simulate a slide mass traveling down a long slope into deep water, large deep water (short) waves often are generated, and simulations crashed. The solution to this problem was use of the two-layer model. The two-layer model has accuracy into much deeper water than the one-layer, and proved to be stable, without production of unrealistic, large short waves. Therefore while the two-layer model is not strictly required for accuracy in the run-up region for any of the simulations presented here, it is required for accuracy/stability in the deep water region, without which the simulations will not successfully complete.

3. Numerical Model

[11] The finite difference algorithm presented by *Lynett and Liu* [2002, 2004a] is used to solve the model equations. A high-order predictor-corrector scheme is utilized, employing a third order in time explicit Adams-Bashforth predictor step, and a fourth order in time Adams-Moulton implicit corrector step [*Press et al.*, 1989]. Spatial derivatives are differenced to fourth-order accuracy, yielding a model which is numerically accurate to $(\Delta x)^4$, $(\Delta y)^4$ in space and $(\Delta t)^4$ in time.

[12] Run-up and run-down of the waves generated by the landslide disturbance will be examined. The moving boundary scheme employed here is the technique developed by *Lynett et al.* [2002]. Founded around the restrictions of the high-order numerical wave propagation model, the moving boundary scheme utilizes linear extrapolation of free surface and velocity through the shoreline, into the dry region. This approach allows for the five-point finite difference formulas to be applied at all points, even those neighboring dry points, and thus eliminates the need of conditional statements.

4. Landslide Description

4.1. Slide Motion

[13] All of the simulations undertaken for this study use a solid slide mass traveling down an infinite slope. When fully submerged, the slide motion is described by the formulation given by *Watts* [1997]. This formulation requires the specification of a number of coefficients, and those used in this paper are identical to the set employed by *Grilli and Watts* [1999].

[14] Many of the simulations performed, however, are for initially subaerial slides. The expression for slide velocity must be altered to include the aerial acceleration. The

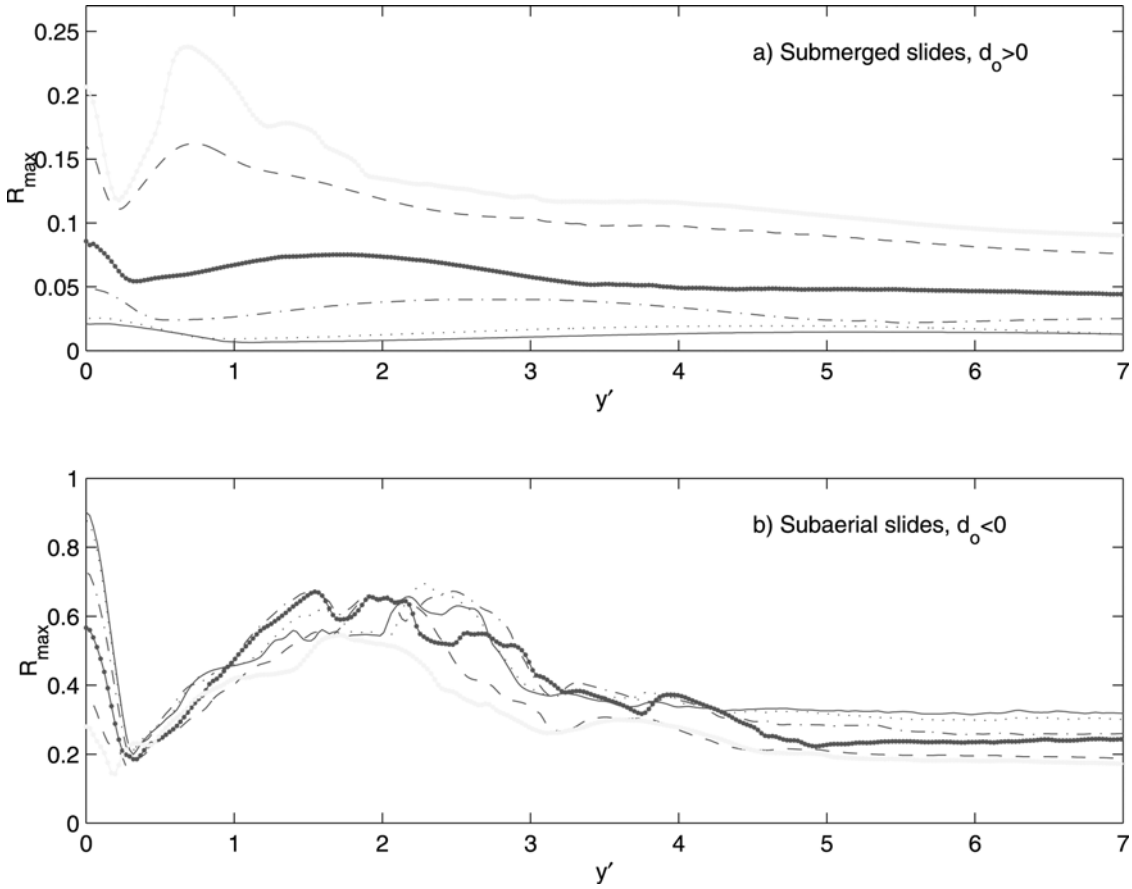

Figure 4. Maximum shoreline elevation at a function of distance from slide centerline for slides with variable ϵ values. The different line types correspond to different ϵ values: [0.125, −0.125] (solid line); [0.15, −0.15] (dotted line); [0.25, −0.25] (dash-dotted line); [0.4, −0.4] (dark bold line); [0.75, −0,75] (dashed line); and [1.0, −1.0] (light bold line). See color version of this figure in the HTML.

approach taken here is to formulate the slide velocity as a weighted average of the aerial and submerged velocity, where the weighting is based on the fraction of the landslide submerged. Thus the slope-parallel velocity of the slide is given by

$$f_s u_s + f_a g t \sin\theta, \tag{1}$$

where g is gravity, t is the time, and θ is the slope angle. The coefficients f_s and f_a represent the volume fractions of the landslide submerged and aerial, respectively, and of course must fall between 0 and 1, summing to 1. The time-dependent velocity of a submerged landslide, u_s, is calculated as by *Grilli et al.* [2002]:

$$u_s = u_t \tanh\left(\frac{t}{t_0}\right), \tag{2}$$

where

$$u_t = \sqrt{gb\frac{\pi(\gamma-1)}{2C_d}\sin\theta}, \tag{3}$$

$$t_0 = u_t \frac{\gamma + C_m}{g(\gamma-1)\sin\theta}, \tag{4}$$

$C_d = C_m = 1$ are the drag and added mass coefficients, respectively, γ is the specific gravity of the slide material, and b is the slope-parallel slide length.

4.2. Landslide Geometry

[15] The graphical definitions of the variables described in this section are shown in Figure 1. The spatial profile of the time-variable seafloor can be given in the general form

$$h(x,y,t) = h_o(x) - h_S(x,t)G(y), \tag{5}$$

where h_o is the planar "baseline" profile with slope angle θ, h_S is the shore-normal profile of the sliding mass, and G is a specified transverse (shore-parallel) profile. The shore-normal profile is similar to that proposed by *Lynett and Liu* [2002]:

$$h_S(x,t) = \Delta h \frac{\left[1+\tanh\left(\frac{x-x_l(t)}{S_l}\right)\right]\left[1-\tanh\left(\frac{x-x_r(t)}{S_r}\right)\right]}{\left[1+\tanh\left(\frac{b\cos\theta}{2S_l}\right)\right]\left[1-\tanh\left(-\frac{b\cos\theta}{2S_r}\right)\right]}, \tag{6}$$

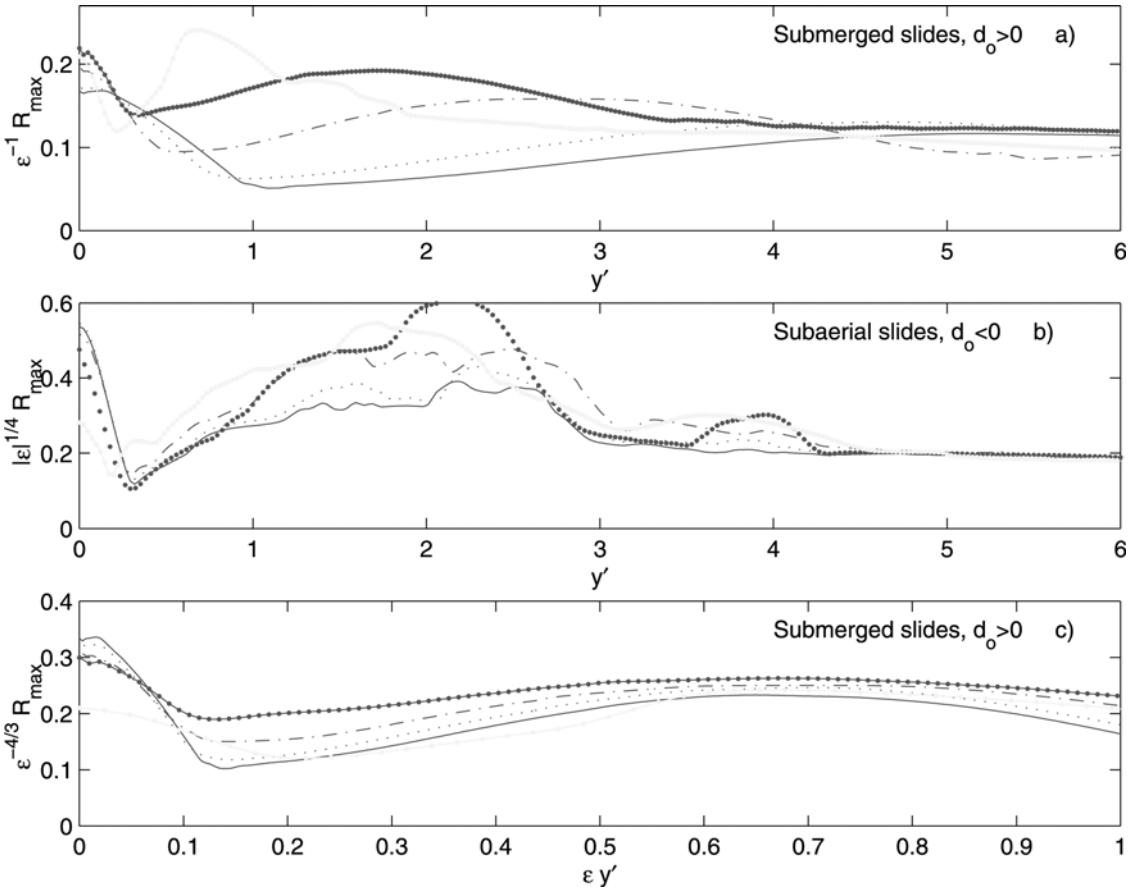

Figure 5. Various trends of the maximum run-up for slides with variable ϵ values. Figure setup is the same as in Figure 4. See color version of this figure in the HTML.

where Δh is the maximum vertical height of the slide, x_l is the location of the tanh inflection point of the left side of the slide, x_r is the location of the inflection point on the right side, b is the constant in time, slope-parallel distance between the inflection points, and S_l, S_r are shape factors controlling the steepness of the left and right slide sides. The right and left boundaries, and steepness factors are given by

$$x_l(t) = x_c(t) - \frac{b}{2}\cos\theta \qquad x_r(t) = x_c(t) + \frac{b}{2}\cos\theta, \tag{7}$$

where x_c is the horizontal location of the center point of the slide, determined using (1). Shown in Figure 1 are typical slide shapes created by the above formulation. It is remarked that the slightly awkward form of (6) is employed so that the effects of slide asymmetry, which can be altered through S_l and S_r, can be examined.

[16] For the transverse profile, a Gaussian is employed:

$$G(y) = \exp\left[-\left(\frac{y - y_o}{0.23W}\right)^2\right], \tag{8}$$

where y_o is the centerline coordinate of the slide, W is the width of the slide, defined as the distance between locations where the vertical slide thickness is 1% of the maximum thickness. For the simulations to be presented in the following sections, there are eight parameters to be varied. (1) Parameter Δh is the maximum vertical thickness of the slide. (2) Parameter d_o is the vertical distance from the center point of the slide to $z = 0$ at time $t = 0$; positive for the submerged slides and negative for the subaerial slides presented here. (3) Parameters l_F, l_B are the horizontal length of the front slide side (forward facing) and the back slide side, respectively, in the shore-normal direction; defined as the distance from the location of maximum vertical slide thickness, Δh, to the location where vertical slide thickness is $0.01\Delta h$. These lengths are varied through changing S_l and S_r. (4) Parameter $L = l_f + l_B$ are the total horizontal length of the slide in the shore-normal direction. Additionally, we define a wave number for the slide, k_S, such that $k_S = 2\pi/L$. (5) Parameter W is the horizontal width of the slide in the shore-parallel direction. Defined as the distance between locations where the vertical slide thickness is $0.01\Delta h$. (6) Parameter ρ_S is the density of the landslide material. (7) Parameter θ is the slope angle of the "baseline" depth profile. Within this dimensional set, six characteristic dimensionless parameters are defined. (1) Parameter $\epsilon = \Delta h/d_o$ is the dimensionless slide thickness. This parameter is related to the dimensionless amplitude of the generated wave, and thus is an indicator of the importance of shallow water nonlinearity. (2) Parameter $\kappa = l_F/l_B$ is the ratio of the front and back slide lengths. Within this value is a measure of the shape, or symmetry of the slide mass, where a value of 1 represents a symmetric slide in the horizontal plane.

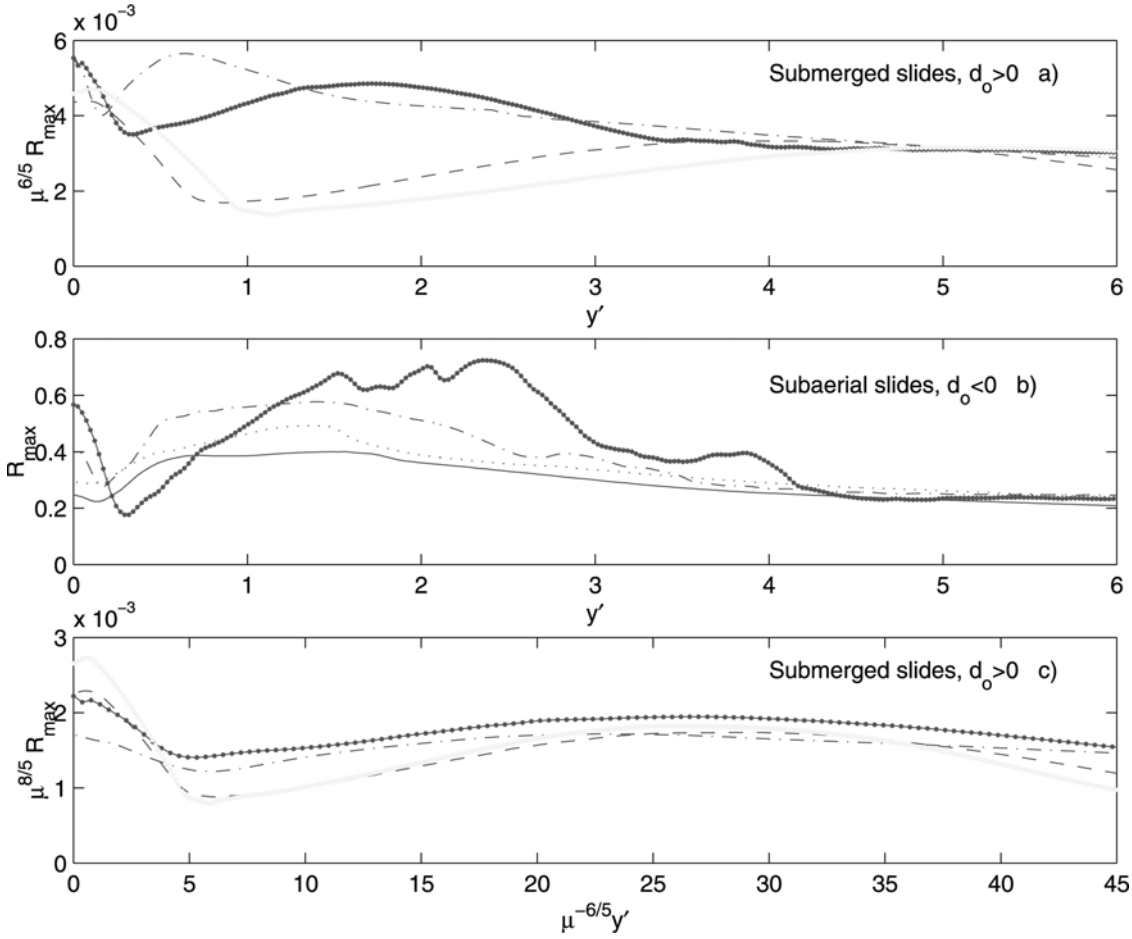

Figure 6. Scaled maximum shoreline elevation at a function of distance from slide centerline for slides with variable μ values. The different line types correspond to different μ values: [0.01] (solid line); [0.025] (dotted line); [0.05] (dash-dotted line); [0.10] (dark bold line); [0.20] (dashed line); and [0.25] (light bold line). Note that each subplot does not contain all line types. See color version of this figure in the HTML.

(3) Parameter $\mu = k_S \Delta h$ is a measure of the steepness of the slide. Constructed as such to carry a relevance to the steepness of a water wave, ka. (4) Parameter $A = L/W$ is the aspect ratio of the slide. (5) Parameter $\gamma = \rho_S/\rho_{water}$ is the specific gravity of the landslide material. (6) Parameter $S = \tan\theta$ is the slope of planar beach. Each of these dimensionless parameters will first be varied independently, and the individual effects of each on the 2HD run-up profile will be discussed. The accuracy restrictions given by *Lynett and Liu* [2002] can be expressed in terms of the above parameters, and require

$$\mu\left(\max\left[\kappa, \frac{1}{\kappa}\right] + 1\right)\left(\frac{1}{\epsilon} + 1\right) \leq \frac{4\pi}{7}. \tag{9}$$

Additionally, slides with large ϵ (relatively small d_o) are not simulated. These are submerged slides that are initially nearly penetrating the still water surface, and numerical simulations indicated that turbulent effects were likely very important. Note that for this analysis, all of the slides denoted "subaerial" are characterized by $d_o < 0$, while all "submerged" slides have $d_o > 0$. The large ϵ slides represent a transitional class of slides between the submerged and subaerial slides simulated in this paper.

5. Two Horizontal Dimension Run-Up Created by Submerged and Subaerial Landslides

[17] Before analyzing the individual effects of the dimensionless parameters through groups of simulations, a single simulation is examined with

$$\epsilon = 0.4, \quad \kappa = 1.0, \quad \mu = 0.01, \quad A = 1.0, \quad \gamma = 2.0, \quad S = 1/10.$$

The above ϵ indicates that nonlinear effects are likely important, μ tells that this slide is thin (or long), and the slope is relatively steep, although still in the validity range of the depth-integrated model used here. This simulation, as well as all to be discussed, employed a spatial domain that was large enough such that reflections off the side walls do not affect any of the results presented. Eight spatial snapshots of the free surface elevation, ζ, are plotted in Figure 2. As the slide motion initiates, at $t\sqrt{gd_o}/L = t' = 0.3$,

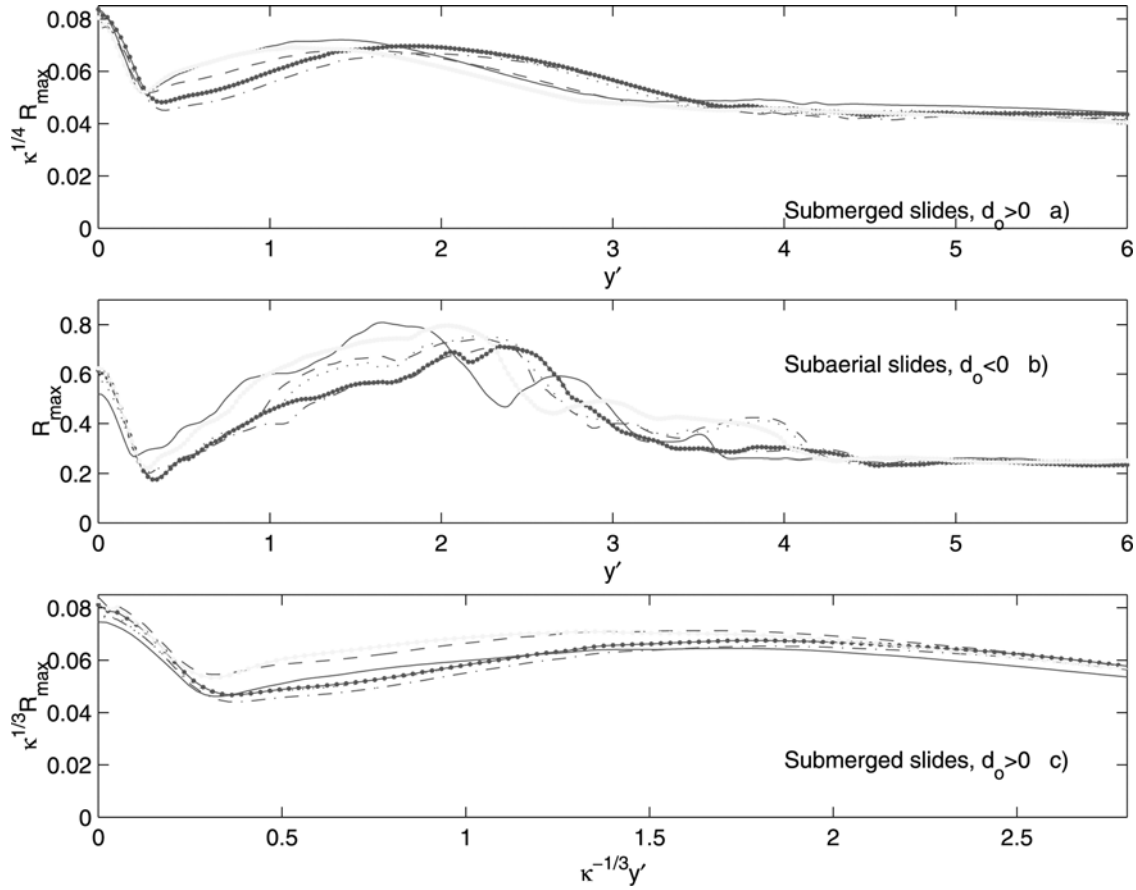

Figure 7. Scaled maximum shoreline elevation at a function of distance from slide centerline for slides with variable κ values. The different line types correspond to different κ values: [1.7] (solid line); [1.2] (dotted line); [1.1] (dash-dotted line); [0.90] (dark bold line); [0.83] (dashed line); and [0.73] (light bold line). See color version of this figure in the HTML.

an elevation wave is generated and traveling offshore, while the depression wave created by the landward slide face is already interacting with the shoreline. As the slide continues into deeper water, the offshore directed waves develop into a oscillatory train, trailed by short waves resembling a "V." By $t' = 1.0$, edge waves begin to dominate the wave field near the shoreline. These trapped waves exhibit their characteristic dispersive behavior, as the longer waves travel away from $y = 0$ quickly, leaving a dispersive tail of shorter waves behind. It is clear from this simulation that 2HD effects can be extremely important to the accurate prediction of landslide generated shoreline movement.

[18] The complete picture of shoreline motion for this simulation is shown in Figure 3. This figure gives the shoreline elevation as a function of time for all y' shoreline locations. At the earliest times, $t' < 0.2$, the only section of shoreline experiencing water motion is that directly landward of the slide due to the back face–generated depression wave. The front face elevation wave quickly wraps around the depression such that immediately outside of the slide centerline (i.e., $y' > 0.5$), shoreline motion is characterized by a leading elevation wave. Progressing further in time, the edge waves lead to numerous significant oscillations of the shoreline, for example there are a series of large run-up maxima near $y' = 3$, with the third being the largest (run-up time series are also shown in Figure 3). This is in interesting contrast to the location where one might expect the motion to be most extreme; at $y' = 0$ there is only a single elevation peak, with a magnitude less than that for $1 < y' < 5$. Again, 2HD effects, in particular edge wave formation, drive maximum run-up patterns.

[19] The occurrence of trapped energy in edge waves will lead to a division of the near and far fields. Here, the far field is defined as the region displaced from the projection of the landslide, on the nearby beach, where edge waves become important. The near field is the region where the wave field is dominated by source-specific waves. These source-specific waves are those which, if the landslide was away from the beach, would radiate out from the source and decay rapidly due to amplitude spreading. Radially spreading source waves are expected to exhibit amplitude decay proportional to $1/r^{4/3}$ [*Mei*, 1983], where r is the scaled radial distance from the source. As edge waves are trapped with little decay, it is expected that the near-far field division occurs around $r \approx 5$, or five slide widths from the source, where the near field amplitude has decreased to approximately 10% of its

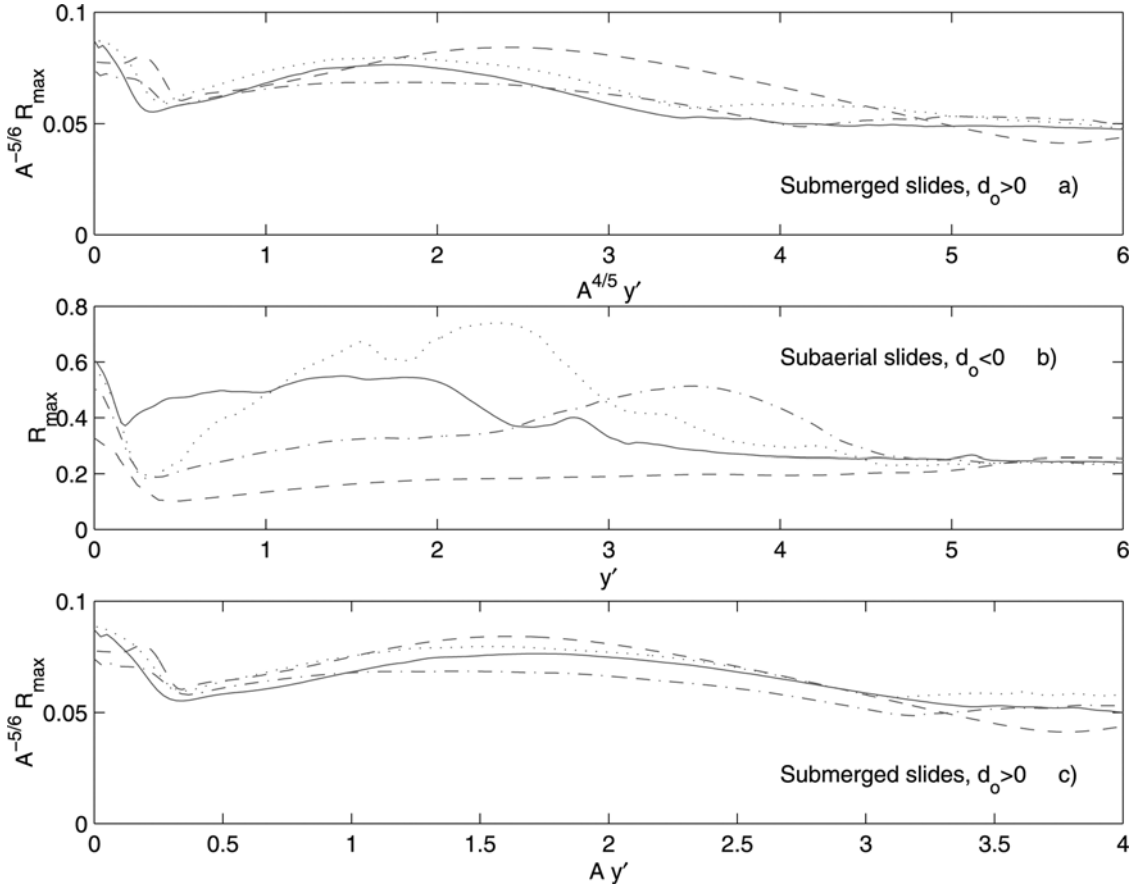

Figure 8. Scaled maximum shoreline elevation at a function of distance from slide centerline for slides with variable A values. The different line types correspond to different A values: [1] (solid line); [2] (dotted line); [5] (dash-dotted line); and [10] (dashed line). See color version of this figure in the HTML.

maximum. It will be demonstrated in this paper that the division does in fact occur roughly five length scales from the source.

[20] In the following subsections, the 2HD dependance on six dimensionless parameters is examined.

5.1. Variable $\epsilon = \Delta h/d_o$: Dimensionless Slide Thickness

[21] Here ϵ is varied through the range $0.125 < |\epsilon| < 1.0$, for both positive and negative ϵ values. The parameters which are constant for all of these simulations are

$$\kappa = 1.0, \quad \mu = 0.1, \quad A = 1.0, \quad \gamma = 2.0, \quad S = 1/10.$$

The dimensionless maximum shoreline elevations or run-ups, R_{max}, as a function of distance from the slide centerline for both submerged and subaerial landslides are given in Figures 4a and 4b, respectively. The dimensional run-up has been scaled by Δh to yield R_{max}. For the submerged slides, there is a clear trend of decreasing R_{max} with decreasing ϵ. This is not the case for the subaerial slides, as from roughly $y' = 0.5$ to 4.0, the curves fall very close together. The secondary maximum in run-up, which is due to edge wave formation, occurs between $y' = 1.5$ to 2.5 with a magnitude $0.55 < R_{max} < 0.65$ for the subaerial slide range tested here.

[22] Now, trends within the run-up profiles are sought. As there is only one variable parameter, ϵ, for all the simulations in Figure 4, it must be used in any attempt to condense the data into single trends. First, the submerged run-up profiles in Figure 4a were multiplied by the factor $1/\epsilon$; this modified plot is given as Figure 4a. While no unique trend could be achieved across the range $0.1 < y' < 4.5$, it is evident that the maximum run-up directly landward of the slide ($y' \approx 0$) falls in the range $0.18 < R_{max}/\epsilon < 0.21$. Perhaps more interesting is that all of the run-up profiles condense into a single trend for $y' > 4.5$. This trend is very slowly decreasing, with a mean value of $R_{max}/\epsilon \approx 0.11$. The subaerial slide run-up can also be condensed for $y' > 4.5$. Shown in Figure 4b is R_{max} multiplied by $\epsilon^{1/4}$. The result is a very high correlation trend for $y' > 4.5$ such that $R_{max}\epsilon^{1/4} = 0.2$. These two data manipulations strongly indicate that there is a transition near $y' = 4.5$, where for lesser values an accurate description of the source is extremely important, but for values larger, not important at all. Thus $y' \approx 4.5$, or 4.5 slide widths from the centerline, likely divides the near and far fields.

[23] For a final analysis of these simulations, the submerged slide profiles are once more examined. By multiplying y' by ϵ, all of the secondary run-up peaks, a result of the edge waves, occur at the same location of $\epsilon y' \approx 0.7$, with a magnitude $0.22 < R_{max}/\epsilon^{4/3} < 0.26$. This data is shown in Figure 5c. This result indicates that even in the very near

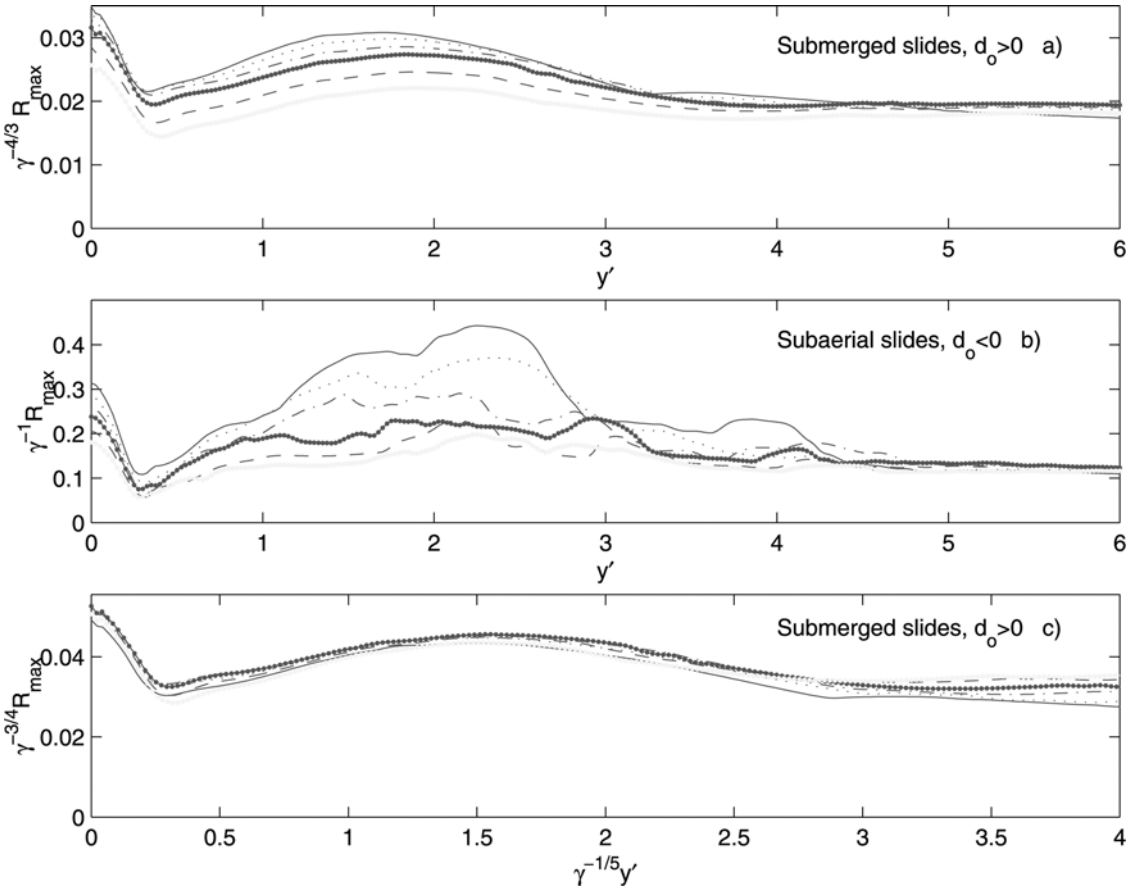

Figure 9. Scaled maximum shoreline elevation at a function of distance from slide centerline for slides with variable γ values. The different line types correspond to different γ values: [1.8] (solid line); [2.0] (dotted line); [2.2] (dash-dotted line); [2.4] (dark bold line); [2.8] (dashed line); and [3.2] (light bold line). See color version of this figure in the HTML.

field area, where nonlinear and dispersive effects are important, certain aspects of the slide behavior will follow simple scaling laws.

5.2. Variable $\mu = k_S\Delta h$: Slide Steepness

[24] Now μ is varied through the range $0.01 < \mu < 0.25$. The parameters which are constant for all of these simulations are

$$\epsilon = \mp 0.4, \quad \kappa = 1.0, \quad A = 1.0, \quad \gamma = 2.0, \quad S = 1/10.$$

The μ range for submerged slides is $0.05 < \mu < 0.25$, due to the fact that $x_o/L < 0.5$ for lesser values. For subaerial slides the range is $0.01 < \mu < 0.1$; larger μ values tended to generate very steep waves which one would expect to break in a physical setup. The scaled dimensionless maximum shoreline elevations or run-ups, $R_{\max}$, as a function of distance from the slide centerline for both submerged and subaerial landslides are given in Figure 6. Note that this figure is constructed in an identical fashion as Figure 5. Again, there is a far field collapse of the run-up curves for $y' > 4.5$ for both submerged and subaerial slides, shown in Figures 6a and 6b, where the submerged run-up has been scaled by $\mu^{6/5}$. There is no factor required for the subaerial run-up, indicating that far field run-up has no dependence on μ. In Figure 6c, the submerged run-up is scaled by $\mu^{8/5}$ and the distance by $\mu^{-6/5}$, yielding the relationship that the secondary run-up peak occurs near $y' \approx 28\mu^{6/5}$ with a magnitude of $R_{\max} \approx 0.0018\ \mu^{-8/5}$.

5.3. Variable $\kappa = l_F/l_B$: Symmetry of Slide Shape

[25] In this section, κ is varied through the range $0.7 < \kappa < 1.7$. Note that a small κ value indicates a relatively steeper front face, which is a situation commonly found with deformable landslide flows. The parameters which are constant for all of these simulations are

$$\epsilon = \mp 0.4, \quad \mu = 0.1, \quad A = 1.0, \quad \gamma = 2.0, \quad S = 1/10.$$

The dimensionless maximum shoreline elevations or run-ups, $R_{\max}$, as a function of distance from the slide centerline for both submerged and subaerial landslides are given in Figure 7. Although there is a clear dependency on κ, the relatively low powers of scalings indicate that the dependency is weak over the range tested. The far field collapse of the run-up for both submerged and subaerial slides is evident again.

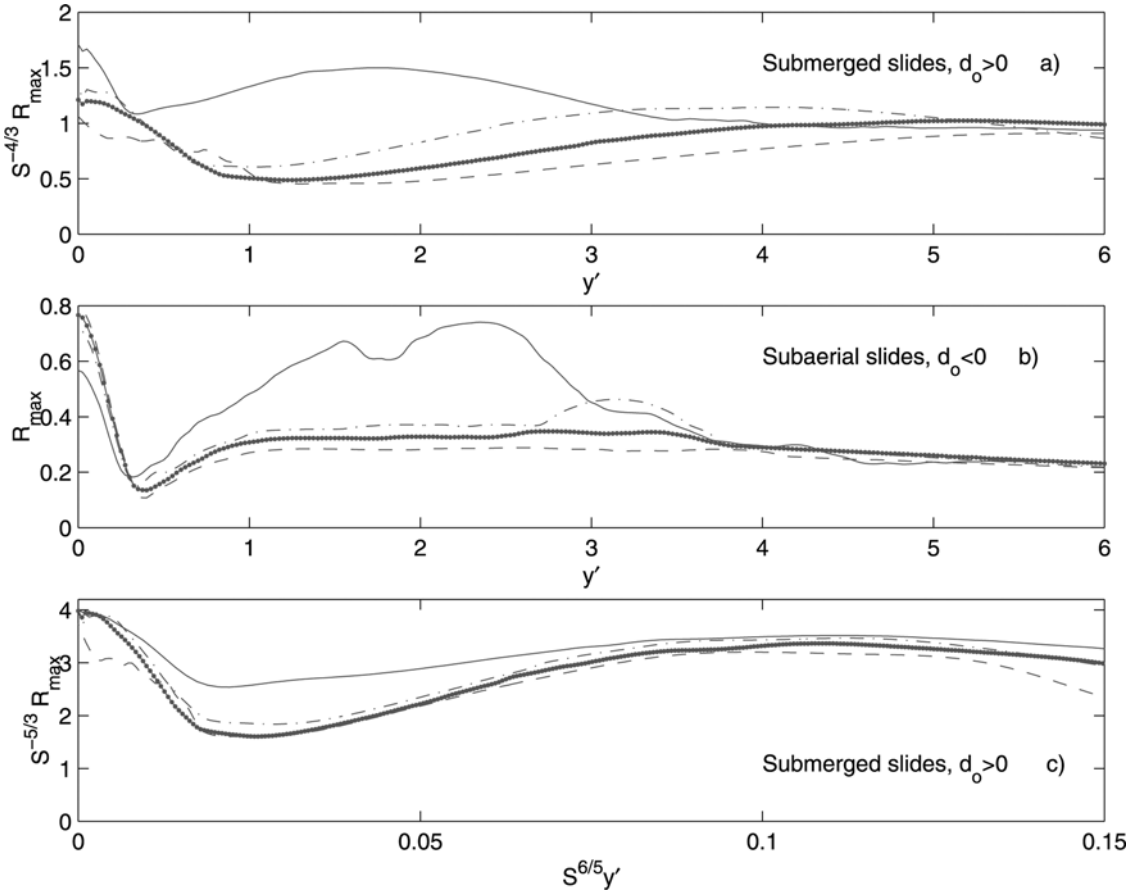

Figure 10. Scaled maximum shoreline elevation at a function of distance from slide centerline for slides with variable S values. The different line types correspond to different S values: [1/10] (solid line); [1/20] (dash-dotted line); [1/25] (dark bold line); and [1/30] (dashed line). See color version of this figure in the HTML.

5.4. Variable $A = L/W$: Aspect Ratio of Slide

[26] Here A is varied through the range $1 < A < 10$. Only values of $A \geq 1$ are tested due to the fact that physical landslides tend to have large A more frequently than small A. Additionally, there is practical limitation, in terms of computer time, on the number of numerical simulations which could be run for very large or small A. This limitation arises from the imposed requirement of a minimum of 20 grid points across the shortest horizontal slide dimension, and thus large or small A simulations require more grid points. The parameters which are constant for all of these simulations are

$$\epsilon = \mp 0.4, \quad \kappa = 1.0, \quad \mu = 0.1 \quad \gamma = 2.0, \quad S = 1/10.$$

The dimensionless maximum shoreline elevations or run-ups, R_{max}, as a function of distance from the slide centerline for both submerged and subaerial landslides are given in Figure 8. The far field collapse of the run-up curves for $y' > 4.5$ for both submerged and subaerial slides is shown in Figures 8a and 8b, where the submerged run-up has been scaled by $A^{-3/5}$. There is no factor required for the subaerial run-up, indicating that far field run-up has no dependence on A.

5.5. Variable $\gamma = \rho_S/\rho_{water}$: Specific Gravity of Slide Material

[27] Next, γ is varied through the range $1.8 < \gamma < 3.2$. The parameters which are constant for all of these simulations are

$$\epsilon = \mp 0.4, \quad \kappa = 1.0, \quad \mu = 0.1, \quad A = 1.0, \quad S = 1/10.$$

The dimensionless maximum shoreline elevations or run-ups, R_{max}, as a function of distance from the slide centerline for both submerged and subaerial landslides are given in Figure 9. Trends from both submerged and subaerial slides converge with a high degree of precision. Of note is that far field subaerial run-up is dependent on γ, which is just the second parameter found to influence this run-up, the other being ϵ.

5.6. Variable $S = \tan\theta$: Beach Slope

[28] Finally, S is varied through the range $1/30 < S < 1/10$. The parameters which are constant for all of these simulations are

$$\epsilon = \mp 0.4, \quad \kappa = 1.0, \quad \mu = 0.1, \quad A = 1.0, \quad \gamma = 2.0.$$

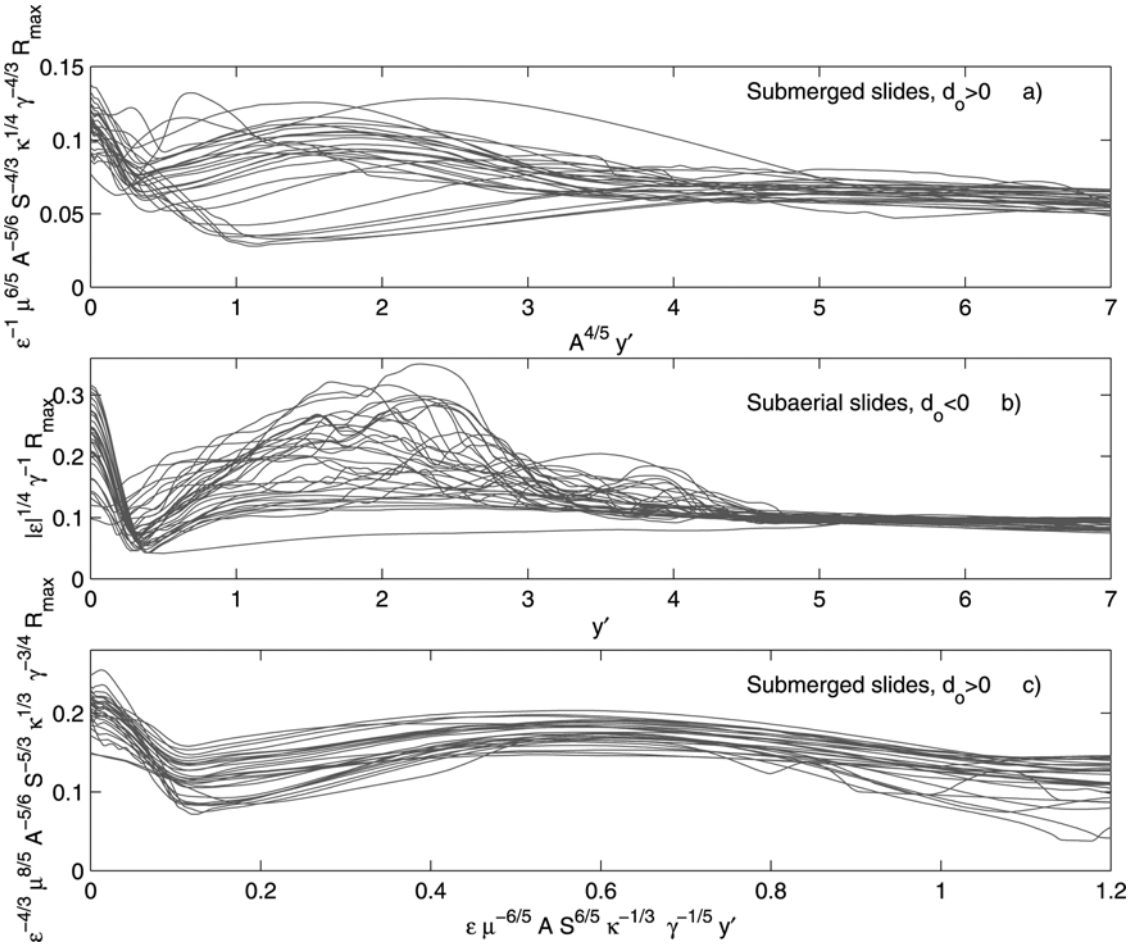

Figure 11. Scaled maximum shoreline elevation as a function of distance from slide centerline for all slides. See color version of this figure in the HTML.

The dimensionless maximum shoreline elevations or run-ups, R_{max}, as a function of distance from the slide centerline for both submerged and subaerial landslides are given in Figure 10. The far field collapse of the run-up curves is again evident, where the submerged run-up has been scaled by $S^{-4/3}$. There is no factor required for the subaerial run-up, indicating that far field run-up has no dependence on S, as was the case of all the parameters except ϵ and γ. In Figure 10c, the submerged run-up is scaled by $S^{-5/3}$ and the distance by $S^{6/5}$, yielding the relationship that the secondary run-up peak occurs near $y' \approx 0.11\ S^{-6/5}$ with a magnitude of $R_{max} \approx 3.0\ S^{5/3}$.

5.7. Combined Trends

5.7.1. Far Field

[29] With the parameter dependencies for each of the six sets of numerical experiments described above, we can combine these dependencies to determine global trends. In addition, 18 more simulations were run with dimensionless parameters lying within the ranges examined above, and are included in the plots discussed now. Looking first to the far field behavior of submerged landslide run-up, the scalings shown in Figures 5a, 6a, 7a, 8a, 9a, and 10a are combined, and the resulting plot is given in Figure 11a. For far-field, submerged landslide run-up, the important parameter is

$$C_1 = \epsilon \mu^{-6/5} A^{5/6} S^{4/3} \kappa^{-1/4} \gamma^{4/3}. \tag{10}$$

Examination of Figure 11a shows that C_1 influences the far field aspects of submerged landslide run-up. Looking to the far field, which is reasonably defined as $y' > 5A^{-4/5}$, we see the convergence of run-up curves. This convergence starts with a maximum run-up of $R_{max} = 0.07 \mp 0.015\ C_1$ and decreases slowly, exhibiting decreasing scatter within the trend, reaching $R_{max} = 0.06 \mp 0.01 C_1$ by $y' = 7\ A^{-4/5}$.

[30] For far-field, subaerial landslide run-up, the parameter of interest is

$$C_2 = \epsilon^{-1/4} \gamma. \tag{11}$$

An extremely clear confluence of subaerial run-up curves for $y' > 5$ is shown in Figure 11b. This is an interesting result, indicating that for subaerial slides, the far field run-up can be very closely estimated with only knowledge of the thickness, initial location, slide width, and density. The maximum run-up is $R_{max} = 0.10 \mp 0.01 C_2$ at $y' = 5$, slowly decreasing to $R_{max} = 0.09 \mp 0.01 C_2$ at $y' = 7$.

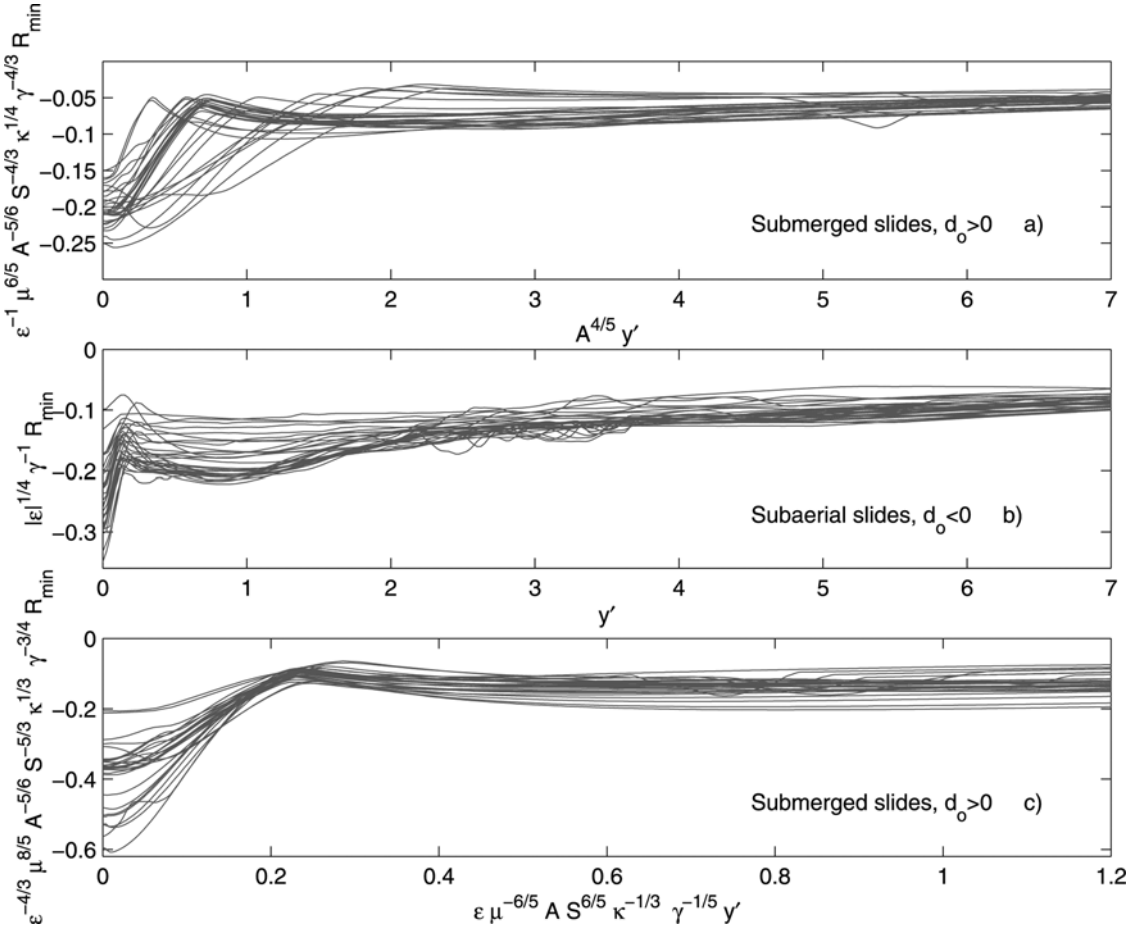

Figure 12. Scaled minimum shoreline elevation as a function of distance from slide centerline for all slides. See color version of this figure in the HTML.

[31] Finally, the secondary run-up peak, due to edge wave propagation, is checked for submerged slides. Here, the important parameters impacting the properties of secondary run-up are

$$C_3 = \epsilon^{4/3}\mu^{-8/5}A^{5/6}S^{5/3}\kappa^{-1/3}\gamma^{3/4} \tag{12}$$

$$C_4 = \epsilon^{-1}\mu^{6/5}A^{-1}S^{-6/5}\kappa^{1/3}\gamma^{-1/5}. \tag{13}$$

With these parameters, the secondary run-up peak can be described approximately as being located at $y' = 0.60 \mp 0.1C_4$, with a magnitude of $R_{max} = 0.17 \mp 0.03C_3$. In general, the error for the predictions presented in this section is roughly ∓15%.

[32] While the entire focus of this paper up to now has been on run-up, run-down can be an equally important, and destructive, aspect of the waves generated by landslides. Applying the scalings found above for run-up, the run-down is given in Figure 12, presented in the same form as Figure 11. Just as with the run-up, we see the far field collapse of the submerged and subaerial run-down, shown in Figures 12a and 12b, at roughly the same shoreline locations. This is an indication that the scalings are in fact a good basic representation of the physical aspects of the landslide problem; they were determined for run-up, but work equally well for run-down.

5.7.2. Near Field

[33] All of the previous analysis examined far field scalings, and the search for asymptotic run-up trends. The entire analysis can easily be repeated in an attempt to uncover the proper run-up scalings for a specific location in the near field. In particular, dimensionless expressions are sought for run-up and run-down at $y' \approx 0$, which for many slide setups will be the location of the largest shoreline movement. Additionally, these $y' \approx 0$ run-up/run-down scalings will allow for comparisons with existing experimental data, and validation of the trend-finding approach utilized here.

[34] Repeating the analysis of sections 5.1–5.6, the run-up at $y' \approx 0$ for submerged slides can be given by $R_{max} \approx 0.30 \mp 0.05C_5$, where

$$C_5 = \epsilon^{1.16}\mu^{-1.40}A^{0.83}S^{1.71}\kappa^{-0.015}\gamma^{0.80}. \tag{14}$$

Run-down for submerged slides is described by $R_{min} \approx -0.23 \mp 0.04C_6$, where

$$C_6 = \epsilon\mu^{-1.19}A^{0.87}S^{1.14}\kappa^{-0.23}\gamma^{0.62}. \tag{15}$$

It is reiterated here that the dimensional run-up and run-down has been scaled by Δh to yield R_{max} and R_{min}. Figure 13 shows the excellent fit for the run-up and run-

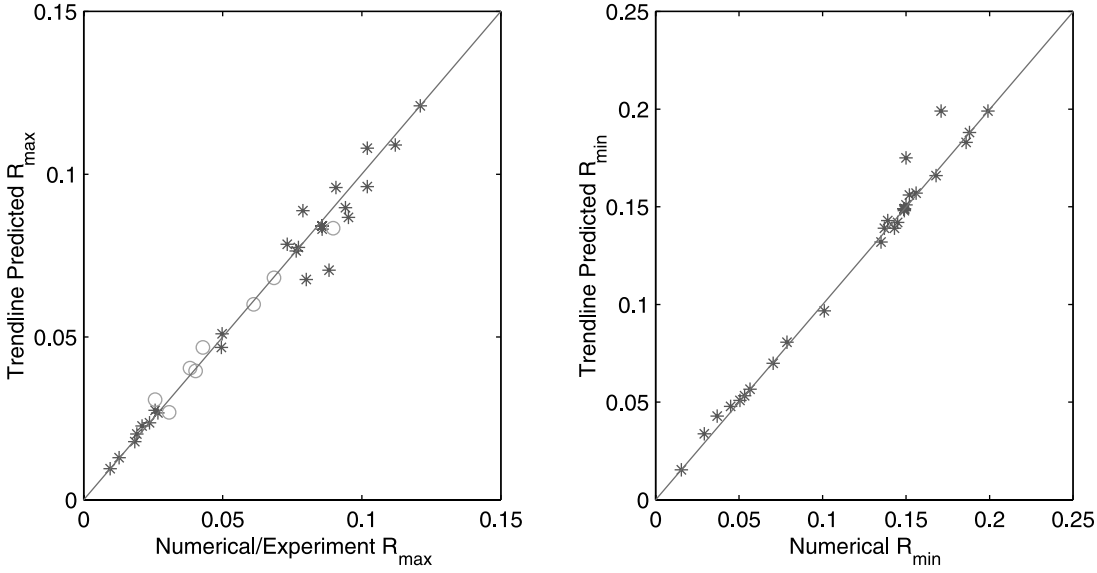

Figure 13. Accuracy of predicted submerged slide run-up/run-down versus results obtained by numerical simulation (asterisks) and experiment (circles). See color version of this figure in the HTML.

down predictions. Also included in the plots are experimental data, discussed in the next section.

6. Comparison With Experimental Data

[35] Owing to the experimental constraints on measuring the three-dimensional (3-D) waves created by landslides, such as accurate measurement of the slide time history and the extremely long and wide tanks required to eliminate reflection effects, very little data exists. Only recently has some data been presented, for example the sliding body experiments of *Synolakis and Raichlen* [2002]. In this paper, some of the data from the *Synolakis and Raichlen* [2002] experiments, where shoreline location was measured, will be employed. For these cases, a spherical hemisphere slid down a 1:2 slope. The hemisphere had a radius of 1.5 ft; the initial depth of submergence and the density of the mass were varied. To be consistent with the work done in this paper, when calculating the length scales of the slide, we look at the horizontal projection of the slide when on the slope. When examining the projection, $L \approx$ 2.6 ft, $\delta h \approx 1.5$ ft, $l_B \approx 1.8$ ft, and $l_F \approx 0.8$ ft.

[36] Table 1 summarizes both the predicted run-up and the measured experimental run-up. Experiment runs 8, 22, and 33 were not included in the comparison, as these cases exhibited significant breaking and turbulence in the laboratory. The predicted run-up is calculated from the scalings developed in this paper: $R_{\max} \approx 0.30 C_5$. The accuracy of the predictions is very good. For the $\gamma = 2.0$ and 2.3 runs, the predictions are excellent. For the $\gamma = 3.2$ runs, the predictions are not quite as good, and are indicative of the error range of the run-up prediction formula. Possible explanations for the decrease in accuracy for larger γ is increased slide bottom friction, or increased level of turbulence due to faster slide motion. These physical aspects are not considered in the numerical model. It should also be noted that the experimental ϵ, μ, κ, and S values are all outside of the range examined numerically in this paper, yet good agreement is still achieved.

[37] Examination of this experimental data provides a good basis for a coefficient and exponent sensitivity analysis. It is reiterated here that, when choosing the exponent values in sections 5.1–5.6, the exponent which provided the least trend line spread was the chosen exponent, thereby pushing the uncertainty into the leading coefficient. For completeness, however, a brief exponent sensitivity analysis will be given now. Looking to the independent parameter analyses (Figures 5–10), the maximum coefficient spread is on the order of $\mp$10%. It is reasonable to assume an exponent spread of the same order for this analysis. Looking to run 9 given in Table 1, the predicted run-up is recalculated, now with all the exponents in C_5 increased and decreased by 10%. Increasing all exponents yields a run-up prediction of 2.7 cm, while decreasing all exponents gives 3.6 cm. This spread is similar to the coefficient uncertainty, $\mp$15%. It is reasonable to state, now, that the maximum possible spread is on the order of $\mp$30%, accounting for possible errors in the leading coefficient and exponents. However, it is expected that much of the

Table 1. Comparison of Maximum Run-Up at $y = 0$[a]

Run	ϵ	γ	Predicted $R_{\max}$, cm	Measured $R_{\max}$, cm	% Error
9	2.3	2.3	3.1	3.1	0
10	1.5	2.3	2.0	2.1	−5
11	1.1	2.3	1.4	1.2	15
23	2.3	3.2	4.1	3.8	10
25	0.8	3.2	1.2	1.4	−15
26	1.1	3.2	1.8	1.8	0
34	2.3	2.0	2.8	2.7	5
35	1.5	2.0	1.8	1.8	0

[a]Predicted data is from the formula $R_{\max} \approx 0.30 C_5$, and experimental data is from *Liu et al.* [2005]. Constant parameters are $\mu = 3.6$, $A = 0.87$, $S = 0.5$, and $\kappa = 0.45$.

spread will be located in the leading coefficient, with an uncertainty of $\mp 15\%$.

[38] In addition to the hemisphere slide experiments compared above, *Liu et al.* [2005] also present wave data for tsunamis generated by triangular block shaped slides. Owing to the sharp corners and very large slopes of these shapes, the Boussinesq-type numerical model is incapable of simulating the triangular block slide. Additionally, comparison of the experimental triangular block slide run-up at $y = 0$ with (14) shows very poor agreement with errors on the order of 100%. As with the hemisphere experiments, ϵ, μ, κ, and S values for the triangular slide are all outside of the range examined numerically in this paper. It must therefore be stated that the trends developed in this paper may only be applicable for smooth shaped slides. In order to simulate these experiments more exactly, a vertically resolving model is required, such as a Navier-Stokes model.

7. Conclusions

[39] A comprehensive set of numerical experiments, including over 75 numerical simulations requiring more than 100 days of desktop CPU time, has been undertaken. The submerged and subaerial slides examined here created nonbreaking waves in shallow to intermediate water. Through analysis of the run-up from these slides, a number of dimensionless relationships have been determined. For submerged slides, the maximum run-up immediately landward of the slide, as well as the magnitude and location of the secondary run-up peak, can now be reasonably estimated. For both subaerial and submerged slides, the division between near and far field has been shown, along with maximum run-up at these locations. In dimensional form, the key relationships are summarized as follows.
(1) Submerged slides:

Maximum run-up immediately landward of slide centerline

$$R/\Delta h \approx 0.30\epsilon^{1.16}\mu^{-1.40}A^{0.83}S^{1.71}\kappa^{-0.015}\gamma^{0.80}; \quad (16)$$

Maximum run-down immediately landward of slide centerline

$$R/\Delta h \approx -0.23\epsilon\mu^{-1.19}A^{0.87}S^{1.14}\kappa^{-0.23}\gamma^{0.62}; \quad (17)$$

Near-far field division

$$y/W \approx 5A^{-4/5}; \quad (18)$$

Run-up at near-far field division

$$R/\Delta h \approx 0.07\epsilon\mu^{-6/5}A^{5/6}S^{4/3}\kappa^{-1/4}\gamma^{4/3}; \quad (19)$$

Location of secondary run-up peak due to edge waves

$$y/W \approx 0.6\epsilon^{-1}\mu^{6/5}A^{-1}S^{-6/5}\kappa^{1/3}\gamma^{-1/5}; \quad (20)$$

Secondary peak run-up

$$R/\Delta h \approx 0.17\epsilon^{4/3}\mu^{-8/5}A^{5/6}S^{5/3}\kappa^{-1/3}\gamma^{3/4}. \quad (21)$$

(2) Subaerial slides:

Near-far field division

$$y/W \approx 5; \quad (22)$$

Run-up at near-far field division

$$R/\Delta h \approx 0.1\epsilon^{-1/4}\gamma. \quad (23)$$

[40] These prediction equations can be expected to have errors bounds of 15%. Comparisons with experiment show that the scaling relationships yield reasonable predictions. These relationships may be useful for preliminary hazard assessment, where a simple and quick estimation of the maximum run-up height and locations are required. Additionally, the formulas developed in this paper will be particulary beneficial to those developing 3-D landslide experiments. Finally, it should be noted that the simulations performed for this paper all make use of a simple planar slope, and do not take into account irregular bathymetry effects. It is known from PNG, as well as from many tsunami events, that bathymetric focusing can greatly impact the shoreline run-up profiles [e.g., *Matsuyama et al.*, 1999], and thus one must always be mindful of site specific seafloor contours when estimating run-up.

[41] **Acknowledgment.** The research reported here is partially supported by grants from the National Science Foundation (CMS-9528013, CTS-9808542, and CMS 9908392).

References

Basterretxea, G., A. Orfila, A. Jordi, B. Casas, P. Lynett, P. L.-F. Liu, C. M. Duarte, and J. Tintoré (2004), Seasonal dynamics of a microtidal pocket beach with Posidonia Oceanica seabeds (Mallorca, Spain), *J. Coastal Res.*, *20*, 1155–1164.

Chang, K. T. (1995), Evolution of landslide-generated edge wave packet, Ph.D. thesis, Univ. of Wash., Seattle.

Gonzalez, F., K. Satake, E. Boss, and H. Mofjeld (1995), Edge wave and non-trapped modes of the 25 April 1992 Cape-Mendocino tsunami, *Pure Appl. Geophys.*, *144*, 409–426.

Grilli, S. T., and P. Watts (1999), Modeling of waves generated by a moving submerged body: Applications to underwater landslides, *Eng. Anal. Boundary Elem.*, *23*, 645–656.

Grilli, S. T., S. Vogelmann, and P. Watts (2002), Development of a 3D numerical wave tank for modeling tsunami generation by underwater landslides, *Eng. Anal. Boundary Elem.*, *26*, 301–313.

Jiang, L., and P. H. LeBlond (1994), Three-dimensional modeling of tsunami generation due to a submarine landslide, *J. Phys. Oceanogr.*, *24*, 559–572.

Liu, P. L.-F. (1994), Model equations for wave propagation from deep to shallow water, in *Advances in Coastal Engineering*, vol. 1, edited by P. L.-F. Liu, pp. 125–157, World Sci., Hackensack, N. J.

Liu, P. L.-F., H. Yeh, P. Lin, K. Chang, and Y.-S. Cho (1994), Generation and evolution of edge-waves packets, *Phys. Fluids*, *10*, 1635–1657.

Liu, P. L.-F., T.-R. Wu, F. Raichlen, C. E. Synolakis, and J. Borrero (2005), Runup and rundown from three-dimensional sliding masses, *J. Fluid Mech.*, in press.

Lynett, P. (2002), A multi-layer approach to modeling nonlinear, dispersive waves from deep water to the shore, Ph.D. thesis, Cornell Univ., Itaca, N. Y.

Lynett, P., and P. L.-F. Liu (2002), A numerical study of submarine landslide generated waves and runup, *Proc. R. Soc. London, Ser. A*, *458*, 2885–2910.

Lynett, P., and P. L.-F. Liu (2004a), A two-layer approach to water wave modeling, *Proc. R. Soc. London, Ser. A*, *460*, 2637–2669.

Lynett, P., and P. L.-F. Liu (2004b), Linear analysis of the multi-layer model, *Coastal Eng.*, *51*, 439–454.

Lynett, P., T.-R. Wu, and P. L.-F. Liu (2002), Modeling wave runup with depth-integrated equations, *Coastal Eng.*, *46*, 89–107.

Lynett, P., J. Borrero, P. L.-F. Liu, and C. E. Synolakis (2003), Field survey and numerical simulations: A review of the 1998 Papua New Guinea tsunami, *Pure Appl. Geophys.*, *160*, 2119–2146.

Matsuyama, M., J. P. Walsh, and H. Yeh (1999), The effect of bathymetry on tsunami characteristics at Sisano Lagoon, Papua New Guinea, *Geophys. Res. Lett.*, *26*, 3513–3516.

Mei, C. C. (1983), *The Applied Dynamics of Ocean Surface Waves*, Wiley-Interscience, Hoboken, N. J.

Nwogu, O. (1993), Alternative form of Boussinesq equations for nearshore wave propagation, *J. Waterw. Port Coastal Ocean Eng.*, *119*, 618–638.

Okal, E., and C. Synolakis (2004), Source discriminants for near-field tsunamis, *Geophys. J. Int.*, *158*, 899–912.

Press, W. H., B. P. Flannery, and S. A. Teukolsky (1989), *Numerical Recipes: The Art of Scientific Computing*, Cambridge Univ. Press, New York.

Ryu, S., M. H. Kim, and P. Lynett (2003), Fully nonlinear wave-current interactions and kinematics by a BEM-based numerical wave tank, *J. Comput. Mech.*, *32*, 336–346.

Schaffer, H., and I. Jonsson (1992), Edge waves revisited, *Coastal Eng.*, *16*, 349–368.

Synolakis, C. E., and F. Raichlen (2002), Wave and run-up generated by a three-dimensional sliding mass, paper 299 presented at the 28th International Conference on Coastal Engineering, Cardiff, Wales, 7–12 July.

Synolakis, C., J. Bardet, J. Borrero, H. Davies, E. Okal, E. Silver, S. Sweet, and D. Tappin (2002), The slump origin of the 1998 Papua New Guinea tsunami, *Proc. R. Soc. London, Ser. A*, *458*, 763–789.

Tinti, S., E. Bortolucci, and A. Armigliato (1999), A numerical simulation of the landslide-induced tsunami of 1988 on Vulcano Island, Italy, *Bull. Volcanol.*, *61*, 121–137.

Ursell, F. (1952), Edge waves on a sloping beach, *Proc. R. Soc. London, Ser. A*, *214*, 79–97.

Watts, P. (1997), Water waves generated by underwater landslides, Ph.D. thesis, Calif. Inst. of Technol., Pasadena.

Wei, G., J. T. Kirby, S. T. Grilli, and R. Subramanya (1995), A fully nonlinear Boussinesq model for surface waves. part 1. Highly nonlinear unsteady waves, *J. Fluid Mech.*, *294*, 71–92.

P. L.-F. Liu, School of Civil and Environmental Engineering, Cornell University, Ithaca, NY 14853, USA. (p113@cornell.edu)

P. Lynett, Department of Civil Engineering, Texas A&M University, College Station, TX 77843-3136, USA. (plynett@tamu.edu)